6.4 IMPROVED CLEAR AIR TURBULENCE DIAGNOSTICS BASED ON ADJUSTMENT DYNAMICS

John A. Knox*
Faculty of Engineering, University of Georgia
Athens, GA

Gary P. Ellrod
Center for Satellite Applications and Research (NOAA/NESDIS)
Camp Springs, MD

Paul D. Williams
Center for Global Atmospheric Modelling, Department of Meteorology, University of Reading, UK

1. INTRODUCTION

During the past four decades, various indices have been developed to help diagnose and forecast the likelihood of high altitude clear-air turbulence (CAT) near the jet stream (e.g. Miles and Howard 1964; Brown 1973; Lee et al 1984; Ellrod and Knapp 1992). These forecast techniques are typically based on parameters derived from upper air or numerical weather prediction model (NWP) data such as vertical wind shear, scalar wind speed, horizontal wind shear, deformation, and the non-dimensional Richardson Number. The NWP indices were designed to attempt to capture grid scale processes that produce the mesoscale (10-100 km) meteorological conditions conducive to sub-grid scale turbulence. Thus, they cannot explicitly forecast turbulence on the scales sensed by aircraft (10-100 m).

In addition to problems related to scale, a significant shortcoming of many of the indices is that they do not account for special situations where unbalanced (i.e. ageostrophic) flow conditions are present**.** Such situations can occur in upper level ridges on the anticyclonic side of the jet stream, as noted by Knox (1997). These non-classical CAT scenarios are characterized by strong vertical and**/**or anticyclonic horizontal wind shears that generate gravity waves through the process of geostrophic adjustment and possibly inertial instability. Gravity waves also typically occur in the exit region of jet streaks (Koch and Dorian 1988), localized maxima within the jet stream core, which are often concurrent with cyclogenesis. The physical process that leads to turbulence in these scenarios is believed to be the modulation of local vertical wind shears by gravity waves, leading to intermittent, strong turbulence over large areas. These areas of turbulence are often characterized by extensive cloud cover, which sometimes contain well-defined transverse cirrus bands that can be observed in satellite visible or infrared (IR) imagery (e.g. Ellrod 1985).

* *Corresponding author address:* John A. Knox, Univ. of Georgia, Faculty of Engineering, Driftmier Engineering Center, Athens, GA 30602; e-mail: jknox@engr.uga.edu

Studies have been conducted to attempt to describe and diagnose unbalanced flow CAT conditions using upper wind or NWP data. Knox (1997) pointed out that in upper flow where strong anticyclonic shear and curvature exist, deformation is small, and turbulence indices based on this parameter as a causative mechanism for CAT are not effective. He showed that in anticyclonic horizontal shear and curvature, the vertical wind shear (principally the ageostrophic component) can greatly exceed that for straight or cyclonic flow conditions, especially as the wind speed approaches the limit of gradient balance, as is often observed in upper-level ridges. These strong vertical shears occur in the presence of weak or even negative absolute vorticity, which is a condition associated with inertial instability in which the value of anticyclonic shear exceeds the Coriolis parameter *f*. These situations are characterized by large values of horizontal divergence and accelerations (Knox 2003).

McCann (2001) evaluated four possible unbalanced flow indicators (and two traditional CAT diagnostics) versus manually filtered aircraft turbulence reports for a large sample of cases (N=1832) from 1 October 1996 to 31 January 1997 to determine which ones related best to turbulence. The indicator with the highest "post-agreement" (one minus the false alarm rate) was the divergence tendency, derived by taking the horizontal divergence of the equation of horizontal motion**.** Further discussion of unbalanced flow diagnostics was provided in Zhang et al. (2000). Some additional model diagnostics that were found to be important include use of the non-linear balance equation, and the Lagrangian Rossby Number, which was employed by Koch and Dorian (1988). This paper describes efforts to improve an existing CAT diagnostic, the deformation - vertical wind shear index (DVSI) (Ellrod and Knapp 1992), by adding a simplified divergence trend term (a proxy for divergence tendency) to account for CAT with unbalanced, anticyclonic jet streams.

2. DATA AND PROCEDURES

Data used to produce the new diagnostic index were obtained from the North American Model (NAM, formerly the ETA) and the 20km resolution Rapid Update Cycle (RUC2). The model data were obtained from the National Centers for Environmental Prediction (NCEP) in Camp Springs, Maryland, a division of the National Oceanic and Atmospheric Administration (NOAA) National Weather Service. The index used as a basis for the experiments was the deformation vertical shear index (DVSI) described by Ellrod and Knapp (1992). The DVSI (originally referred to as TI for Turbulence Index) is:

$$DVSI = [(\delta u/\delta x - \delta v/\delta y)^2 + \delta v/\delta x + \delta u/\delta y)^2]^{1/2} (\delta V/\delta z) \quad (1)$$
$$\text{A} \qquad\qquad \text{B}$$

Term A is resultant deformation (DEF), and B is vertical wind shear of the total vector wind V at each grid point. An additional version of the index (originally referred to as TI2), modified the DVSI to include the presence of horizontal divergence (or convergence) if present. Convergence tended to increase the potential for turbulence through its role in enhancing upper level frontogenesis.

To account for the time variation of divergence present in unbalanced anticyclonic jet streams, a simplified "divergence trend" term (DVT) was obtained:

$$DVT = C\,[(\delta u/\delta x + \delta v/\delta y)_{h2} - (\delta u/\delta x + \delta v/\delta y)_{h1}] \quad (2)$$

The subscripts h1 and h2 represent the 6 hr and 12 hr or 12 hr and 18 hr forecast times, respectively, for the NAM, and the 3 hr and 6 hr forecast times for the RUC2, and C is a constant. The value of C was assigned as 0.1 for both the NAM and RUC to reduce the magnitude of DVT so as not to dominate the DVSI, as DVT can be very large locally, especially in higher resolution mesoscale models such as the RUC2. Negative values of DVT were set to zero.

The DVT was added to the DVSI and run in parallel with the unmodified "operational" version at NESDIS in Camp Springs, Maryland. The DVSI was generated for the 300hPa to 250hPa layer, corresponding to flight altitudes of approximately 30 to 35 thousand ft. The output for both versions of DVSI was displayed as pseudo-color images with aircraft pilot reports (PIREPs) from the previous three hours overlain and were posted on the NESDIS Center for Satellite Applications and Research web server. PIREPs were obtained from NOAA's Family of Services data server. The DVSI images are scaled so that the full range of index values (0 to 16) correspond to an 8-bit brightness count range (0 to 255). Thus, a DVSI value of 12 associated with a high risk of CAT corresponds to a count value of approximately 190. The web address for the DVSI images is: http://www.orbit.nesdis.noaa.gov/smcd/opdb/aviation/tifcsts.html

The divergence-trend-modified DVSI (hereafter, D-DVSI) usually contained some small increases in the background values of the index as a result of the divergence trend term. These variations were filtered out by adjusting the output scale of the image so that DVSI values less than '1' were not displayed in the final image product.

3. EXAMPLES

Two examples of CAT episodes from the winter of 2004-2005 are shown in this section to illustrate the effects of the divergence trend modification to the DVSI. In both cases, the modification resulted in a positive impact on the turbulence forecasts.

3.1 *Case 1: 22 December 2004*

A developing storm system in the Mississippi Valley on 22 December 2004 resulted in extensive cloud cover with embedded convection over the southeastern United States. Figure 1 is a display of grid values of the 12 hr forecast DVSI from the ETA model (now the NAM) for both the DVSI and D-DVSI valid 0000 UTC, 23 December 2004, superimposed on a GOES-12 Infrared (IR) image at 2215 UTC. The maximum DVSI values are approximately doubled in Alabama, Mississippi, northern Georgia, and eastern Tennessee due to the effects of the added DVT term. Figure 2 shows a portion of the pseudo-color image for each product as it appeared on the web site. Red areas are associated with a high risk of CAT (DVSI >12), yellow with a moderate risk, and green with a low risk. Moderate to severe turbulence was reported over eastern Mississippi from 1400-1700 UTC, although PIREPs were infrequent. In addition to the lower Mississippi Valley, other regions where DVSI was enhanced by the addition of DVT were the eastern Gulf of Mexico and the Ohio Valley.

Figure 3 is a 250hPa analysis of radiosondes data valid at 0000 UTC, 23 December 2004. Strong diffluence was evident in the streamlines over the southeastern U. S., which was in the right entrance region of a strong jet stream over the Great Lakes region, and in the left exit region of an approaching jet maximum in the Southern Plains and Southern Rockies. Conceptual models of jet stream dynamics would support strong divergence in the Southeast in this synoptic situation (e.g., Uccellini and Johnson 1979).

Divergence derived from GOES cloud and water vapor motion vectors (Rabin, CIMSS) at 1615 UTC (Figure 4) was quite pronounced, and the water vapor imagery revealed significant cloud bands that were transverse to the flow. Some of these cirrus bands were associated with convective anvils,

while others were non-convective in nature. The transverse bands across northern Alabama have an approximate horizontal wavelength of 80 km, and spatially resemble those identified in satellite imagery in anticyclonic flow during a CAT outbreak by Knox (2001).

3.2 *Case 2: 5 February 2005*

On the morning of 5 February 2005, there was a broad upper level ridge of high pressure over the southern United States in advance of a strong upper trough dropping southward across the Pacific Northwest. Figure 5 displays the 250hPa radiosonde data at 1200 UTC, indicating a strong jet stream along a line from southwest Texas to Oklahoma, Tennessee, and South Carolina. There was no cyclogenesis in progress as with the previous case.

The 18 hr forecast DVSI valid 1800 UTC from the NAM (top panel, Figure 6) showed an axis of maximum CAT risk oriented along the axis of the jet stream. The greatest threat was across Missouri, Kentucky, western North Carolina, and northern South Carolina. The D-DVSI (lower panel, Figure 6) shifted the axis of greatest turbulence risk southward to the anticyclonic side of the jet stream. This newer risk area was better correlated with the turbulence reports observed around that valid time.

A low resolution, color-enhanced GOES IR image (Figure 7) revealed considerable cirrus across the upper ridge, interspersed with well-defined transverse bands, especially in Oklahoma, southern Missouri, and northern Arkansas into Tennessee. A second area of banded cirrus was observed over Colorado, Kansas and Nebraska, and could be associated with a secondary DVSI maximum.

4. SUMMARY OF RESULTS

Based on several months of qualitative comparisons, DVSI maxima in strong anticyclonic flow and curvature were enhanced considerably by the DVT modifications, and related better with turbulence reports in those regions. In other regions, there was no significant change in the index, and thus no negative impacts on its use. As an example to support this finding, Figure 8 is a histogram plot showing the distribution of brightness counts for the 18 hr forecast NAM DVSI image valid 1800 UTC on 22 March 2005. Conditions on this date were similar to those of 22 December 2004, with cyclogenesis in progress due to strong upper trough-jet stream dynamics. The D-DVSI (cyan) is significantly higher than the DVSI (blue) for the brightness count range of approximately 120 to 190, which corresponds to a medium risk of CAT (low risk frequencies are not shown in the histogram). On many days, there were no significant differences between the D-DVSI and DVSI anywhere within the domain of the CONUS and southern Canada. This would be expected in light of the rarity of unbalanced flow conditions.

The greatest benefits so far have been observed using the lower resolution NAM data. The reasons for the differences are not clear, although it is believed that divergence from the RUC2 data is already enhanced through the use of mesoscale aircraft, satellite, and profiler wind data. RUC2 divergence fields are often observed to be quite "noisy," with large small scale variations at the 1hr forecast time. The use of the 3hr and 6hr periods is expected to yield better results.

The use of geostationary satellite imagery remains an excellent tool to diagnose unbalanced flow conditions. Although correlations are not perfect, pronounced transverse cirrus bands are commonly observed in the imagery when unbalanced flow exists. The imagery can thus be used to corroborate model output for these situations.

5. FUTURE WORK

The effectiveness of adding divergence trend to DVSI appears to be promising enough so that permanent implementation is likely prior to the 2005-06 Northern Hemisphere winter, following some additional validation. A more formal method of verification is sought, which will involve direct comparison of aircraft turbulence reports with objective index grid points.

6. NEW DIRECTIONS

An alternative approach to the generation of gravity waves by adjustment processes was pioneered by Ford (1994) based on the theory of the aerodynamic generation of sound waves by Lighthill (1952). Ford's work was recently explored by Williams et al. (2005) using laboratory experiments and model simulations.

Ford's theoretical criterion is derived from taking the curl and divergence of the shallow water momentum equations and combining the results into one equation. As such, it is formally distinct from the dynamical equations upon which the previous discussion of unbalanced modes is based.

The "Lighthill/Ford radiation term" that is the forcing term of Ford's equation is equated with the presence of gravity wave activity. Williams et al. (2005) demonstrated this to be the case using rotating-tank experiments and model simulations of the experiments. The radiation term outperformed horizontal divergence, Richardson number, Brown's (1973) indicator, and Roach's (1970) energy dissipation rate in terms of identifying the

regions of gravity wave activity.

The excellent agreement between the Lighthill/Ford radiation term and the spatial locations of gravity wave emission in the Williams et al. work raises the question: can a version of the Lighthill/Ford expression be developed for operational use in clear air turbulence forecasting? We are currently exploring this possibility, and hope to present additional work on this topic at the meeting.

7. REFERENCES

Brown, R., 1973: New indices to locate clear-air turbulence. *Meteorol. Mag.*, **102**, 347-361.

Ellrod, G. P., 1985: Detection of high level turbulence using satellite imagery and upper air data. NOAA Tech. Memo. NESDIS 10, U. S. Dept. Of Commerce, Washington, DC, 30pp.

Ellrod, G. P., and D. I. Knapp, 1992: An objective clear-air turbulence forecasting technique: Verification and operational use. *Wea. Forecasting*, **7**, 150-165.

Ford, R., 1994: Gravity wave radiation from vortex trains in rotating shallow water. *J. Fluid Mech*., **281**, 81-118.

Knox, J. A., 1997: Possible mechanisms of clear-air turbulence in strongly anticyclonic flow. *Mon. Wea. Rev*., **125**, 1251-1259.

Knox, J. A., 2001: The breakdown of balance in low potential vorticity regions: Evidence from a clear air turbulence outbreak. Preprints, *13th Conference on Atmospheric and Oceanic Fluid Dynamics*, American Meteorological Society, Breckenridge, CO, 64-67.

Knox, J. A., 2003: Inertial instability. In *Encyclopedia of the Atmospheric Sciences*, eds. J. R. Holton, J. Pyle, and J. A. Curry, Academic Press, New York, 1004-1013.

Koch, S. E., and P. B. Dorian, 1988: A mesoscale gravity wave event observed during CCOPE. Part III: Wave environment and probable source mechanisms. *Mon. Wea. Rev*., **116**, 2570-2592.

Lee, D. R., R. S. Stull, and W. S. Irvine, 1984: Clear air turbulence forecasting techniques. Air Weather Service Tech. Note AFGWC/TN-79/001 (REV), Air Force Global Weather Central, Offutt AFB, Nebraska, 16 pp.

Lighthill, M. J., 1952: On sound generated aerodynamically. I: General theory. *Proc. Roy. Soc. London*, **211**, 564-587.

McCann, D. W., 2001: Gravity waves, unbalanced flow, and clear air turbulence. *Nat. Wea. Digest*, **25(1,2)**, 3-14.

Miles, J. W., and L. N. Howard, 1964: Note on a heterogeneous shear flow. *J. Fluid Mech*., **20**, 331-336.

Rabin, R., Cooperative Institute for Meteorological Satellite Studies (CIMSS), University of Wisconsin, Madison: Web site for realtime GOES winds and derived parameters: http://cimss.ssec.wisc.edu/mesoscale_winds/archive.html

Roach, W. T., 1970: On the influence of synoptic development on the production of high level turbulence. *Quart. J. Roy. Meteor. Soc*., **96**, 413-429.

Uccellini, L. W. and D. R. Johnson, 1979: The coupling of upper and lower Tropospheric jet streaks and implications for the development of severe convective storms. *Mon. Wea. Rev*., **107**, 682-703.

Williams, P. D., T. W. N. Haine, and P. L. Read, 2005: On the generation mechanisms of short-scale unbalanced modes in rotating two-layer flows with vertical shear. *J. Fluid Mech*., **528**, 1-22.

Zhang, F., S. E. Koch, C. A. Davis, and M. L. Kaplan, 2000: A survey of unbalanced flow diagnostics and their applications. *Adv. Atmos. Sci.* **17**, 1-19.

8. DISCLAIMER

The contents of this extended abstract are solely the opinions of the authors and do not constitute a statement of policy, decision, or position of the United States Government.

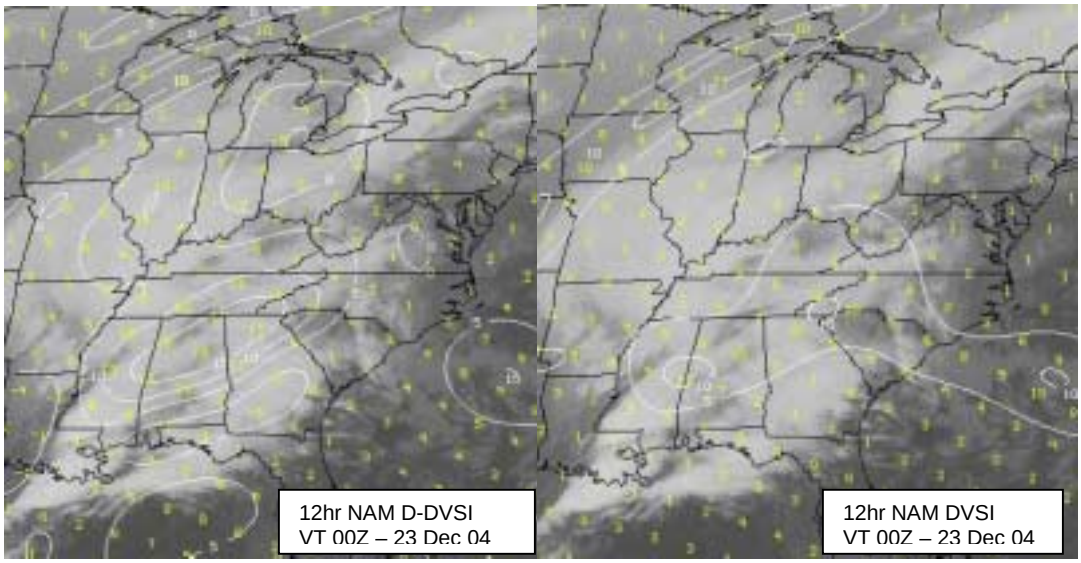

Figure 1. *Gridded data from NAM 12hr forecast valid 0000 UTC, 23 December 2004 for the D-DVSI (left) and the DVSI (right) overlain on a GOES IR image at 2215 UTC, 22 December 2004.*

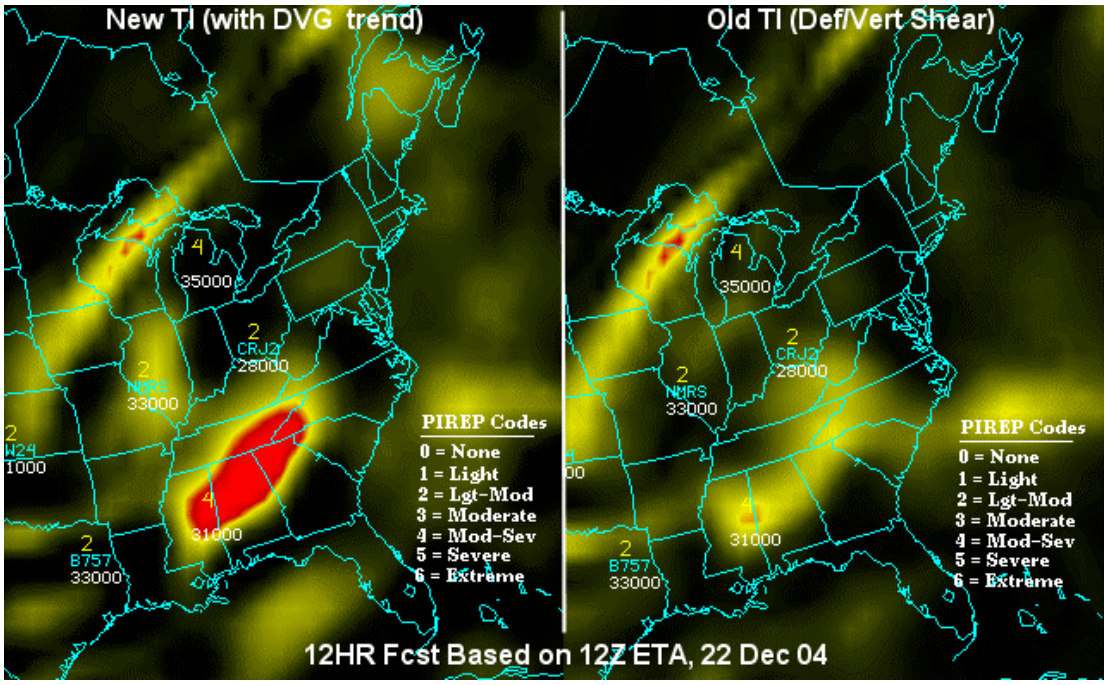

Figure 2. *Pseudo-color image shows D-DVSI (left) and DVSI (right) valid 0000 UTC, 23 December 2004 for the 300hPa to 250hPa layer. Red areas show high risk, yellow medium risk of CAT. Numerical codes of turbulence intensity from PIREPs (yellow), aircraft type (cyan) and altitude (ft-cyan) were obtained from 14-17Z.*

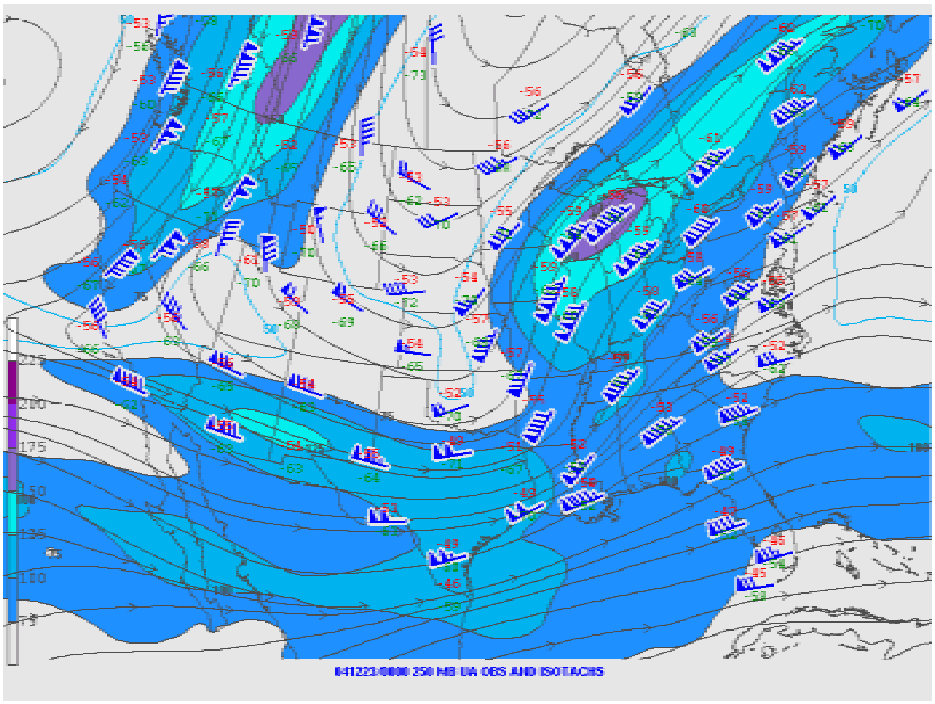

Figure 3. *A 250hPa (mb) analysis is shown valid at 0000 UTC, 23 December 2004. Black contours represent streamlines, and green contours are isotherms (deg C). Plotted winds are in knots (kt), with isotachs greater than 75 kt are highlighted in blue, greater than 150 kt in purple. (Source: NOAA/SPC)*

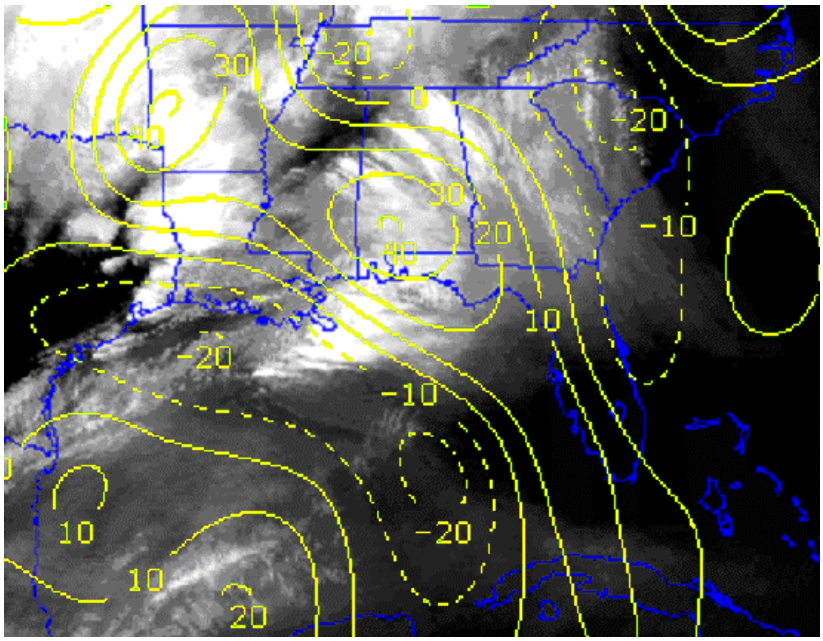

Figure 4. *Upper level divergence (10^{-6} sec^{-1}) derived from GOES cloud motion vectors at 1615 UTC, 22 December 2004, superimposed on a GOES water vapor image. (Obtained from: http://cimss.ssec.wisc.edu/mesoscale_winds/archive.html (R. Rabin, CIMSS))*

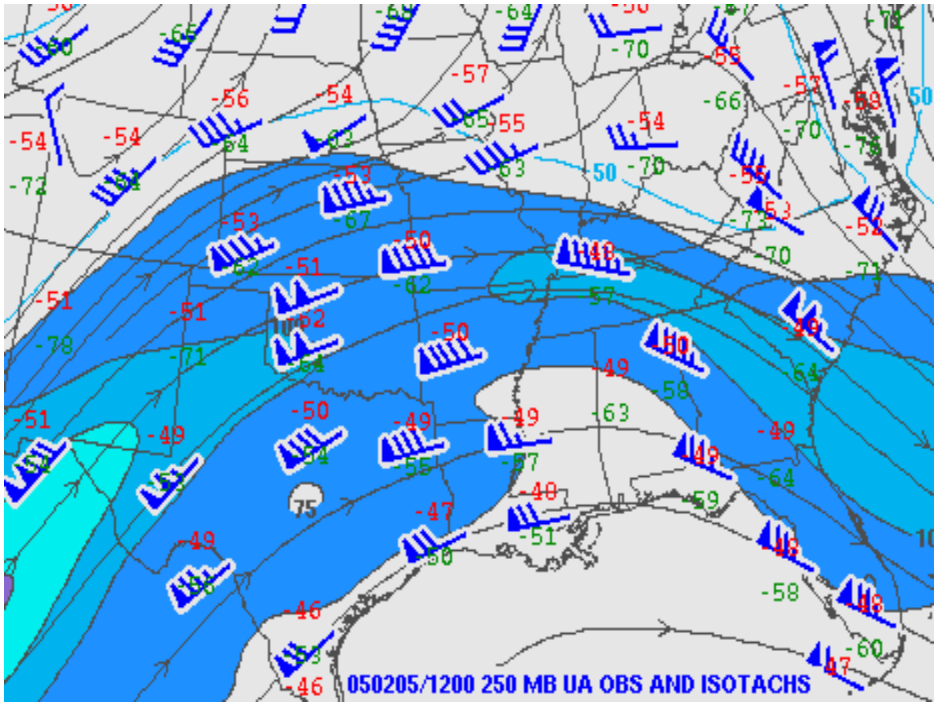

Figure 5. *A 250hPa analysis is shown, valid at 1200 UTC, 5 February 2005. Contours and shading are the same as in Figure 3. (Source: NOAA/SPC)*

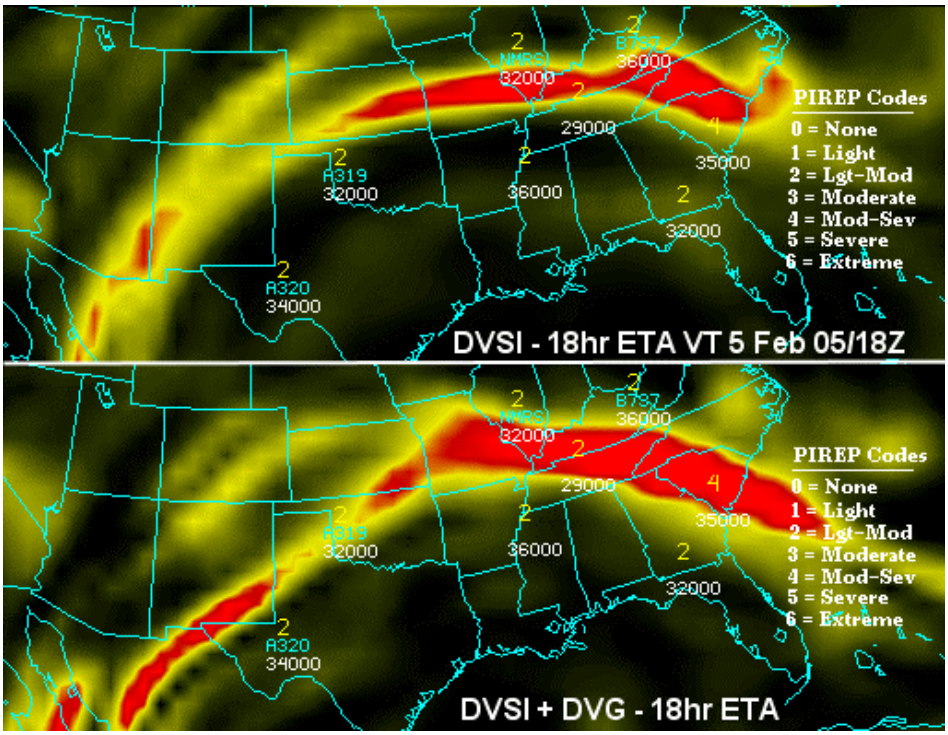

Figure 6. *Pseudo-color image showing 18hr forecast of DVSI (top) and D -DVSI (bottom) for the 300hPa to 250hPa layer, valid 1800 UTC, on 5 February 2005.*

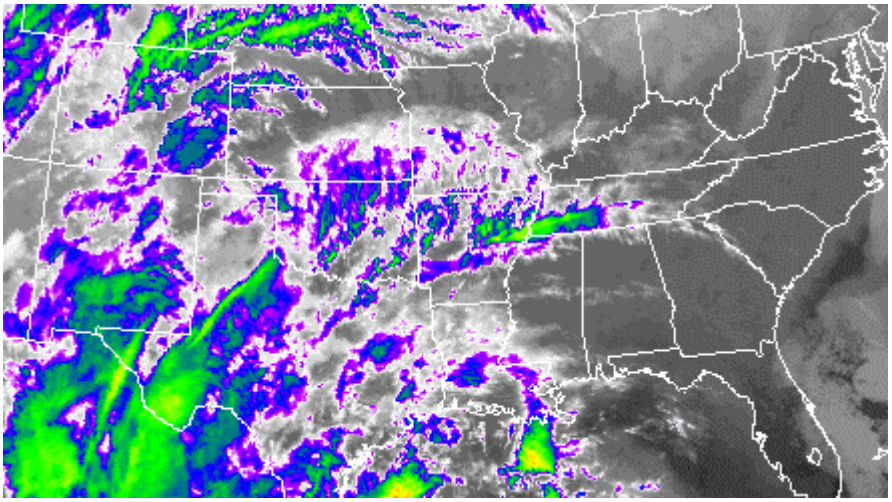

Figure 7. *Color-enhanced GOES-12 IR image at 1615 UTC on 5 February 2005.*

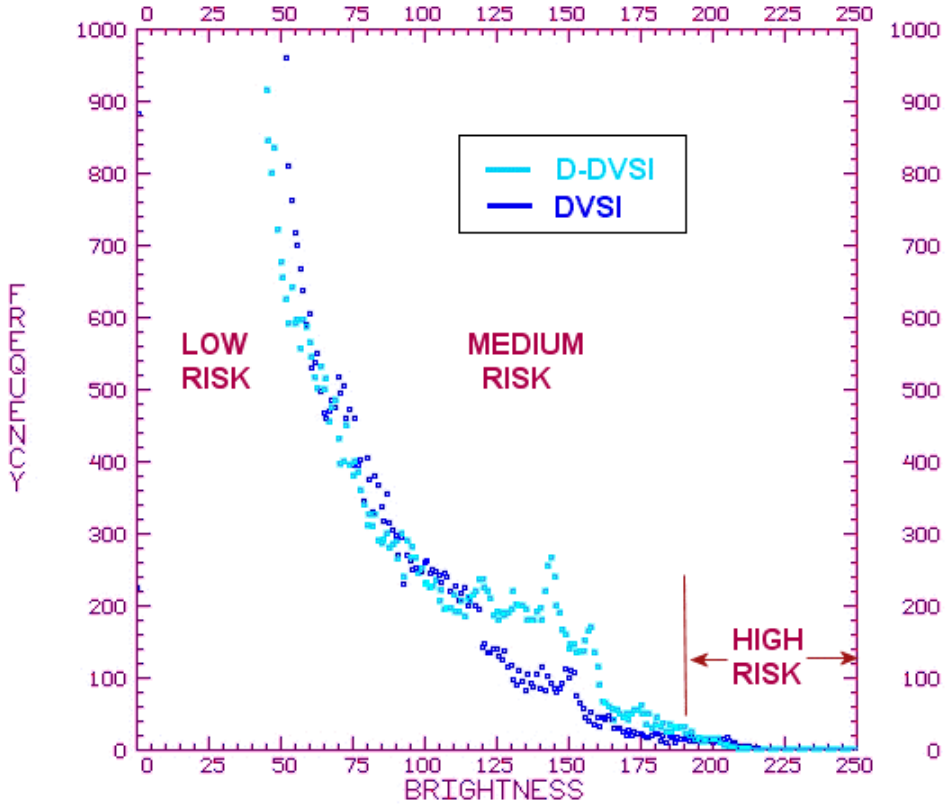

Figure 8. *Histogram of brightness counts from the D-DVSI (cyan) and DVSI (blue) images for the 18 hr NAM forecast valid 1800 UTC, 22 March 2005, for a region that covers the Continental United States, southern Canada, and adjacent coastal waters. A significant increase in frequency was observed for D-DVSI within the brightness range 120 to 190, which is normally associated with a medium risk of CAT. Frequencies for the low risk category are >1000 and are not shown.*